Superconducting Quantum Interference Devices: State of the Art and Applications

REINHOLD KLEINER, DIETER KOELLE, FRANK LUDWIG, AND JOHN CLARKE

Invited Paper

Superconducting quantum interference devices (SQUIDs) are sensitive detectors of magnetic flux. A SQUID consists of a superconducting loop interrupted by either one or two Josephson junctions for the RF or dc SQUID, respectively. Low transition temperature (T_c) SQUIDs are fabricated from thin films of niobium. Immersed in liquid helium at 4.2 K, their flux noise is typically $10^{-6}\Phi_0$ $Hz^{-1/2}$, where $\Phi_0 \equiv h/2e$ is the flux quantum. High-T_c SQUIDs are fabricated from thin films of $YBa_2Cu_3O_{7-x}$, and are generally operated in liquid nitrogen at 77 K. Inductively coupled to an appropriate input circuit, SQUIDs measure a variety of physical quantities, including magnetic field, magnetic field gradient, voltage, and magnetic susceptibility. Systems are available for detecting magnetic signals from the brain, measuring the magnetic susceptibility of materials and geophysical core samples, magnetocardiography and nondestructive evaluation. SQUID "microscopes" detect magnetic nanoparticles attached to pathogens in an immunoassay technique and locate faults in semiconductor packages. A SQUID amplifier with an integrated resonant microstrip is within a factor of two of the quantum limit at 0.5 GHz and will be used in a search for axions. High-resolution magnetic resonance images are obtained at frequencies of a few kilohertz with a SQUID-based detector.

Keywords*—*Flux transformer, gradiometer, Josephson junction, magnetic resonance imaging (MRI), magnetoencephalography (MEG), magnetometer, nuclear magnetic resonance (NMR), superconducting quantum interference device (SQUID).

Manuscript received October 22, 2003; revised February 20, 2004. This work was supported in part by the Director, Office of Science, Office of Basic Energy Sciences, Division of Materials Sciences and Engineering, U.S. Department of Energy under Contract DE-AC03-76SF00098 and in part by the Deutsche Forschungsgemeinschaft.

R. Kleiner and D. Koelle are with the Physikalisches Institut-Experimentalphysik II, Universität Tübingen, Tübingen D-72076, Germany (e-mail: kleiner@uni-tuebingen.de; koelle@uni-tuebingen.de).

F. Ludwig is with the Institut für Elektrische Messtechnik und Grundlagen der Elektrotechnik, Technical University Braunschweig, Braunschweig D-38106, Germany (e-mail: f.ludwig@tu-bs.de).

J. Clarke is with the Department of Physics, University of California, Berkeley, CA 94720-7300 USA and also with the Materials Sciences Division, Lawrence Berkeley National Laboratory, Berkeley, CA 94720-7300 USA (e-mail: jclarke@physics.berkeley.edu).

Digital Object Identifier 10.1109/JPROC.2004.833655

I. INTRODUCTION

Superconducting quantum interference devices (SQUIDs) are very sensitive detectors of magnetic flux. They combine the physical phenomena of flux quantization [1] and Josephson tunneling [2]. Flux quantization requires that the magnetic flux enclosed by a superconducting loop be quantized in units of the flux quantum $\Phi_0 \equiv h/2e \approx 2.07 \times 10^{-15}$ Tm^2. Here, $h \equiv 2\pi\hbar$ is Planck's constant and e is the electron charge. The Josephson effect involves the coherent tunneling of Cooper pairs through a thin barrier separating two superconductors. For currents below a critical value, the pair tunneling constitutes a supercurrent, and no voltage is developed across the junction; a voltage appears for currents greater than the critical value.

There are two kinds of SQUIDs. The first, the dc SQUID [3], consists of two Josephson junctions connected in parallel on a superconducting loop and is operated in the voltage state with a current bias. When the flux in the loop is increased, the voltage oscillates with a period Φ_0. By detecting a small change in the voltage one is able to detect a change in flux typically as low as $10^{-6}\Phi_0$. The second kind, the RF SQUID [4], consists of a single Josephson junction inserted into a superconducting loop. The loop is inductively coupled to the inductor of an *LC*-resonant circuit that is excited with a current at a frequency ranging from a few tens of megahertz to several gigahertz. The amplitude of the oscillating voltage across the resonant circuit is periodic in the applied flux, with a period Φ_0, enabling one to detect changes in flux of the order of $10^{-5}\Phi_0$. The majority of SQUIDs are made of the low transition temperature (T_c) superconductor Nb and operated at or below the boiling point of liquid helium, 4.2 K. The advent of high-T_c superconductors [5], however, led to a worldwide effort to develop devices made of thin films of these materials, resulting in a successful technology. As a result, there are a number of applications involving SQUIDs made from $YBa_2Cu_3O_{7-x}$ (YBCO) operating at or near the boiling point of liquid nitrogen, 77 K.

This paper briefly reviews the theory, fabrication, design, operation, and applications of SQUIDs. Section II provides a short summary of the theory of the dc and RF SQUID, and Section III summarizes the fabrication of low- and high-T_c devices. Section IV describes the configuration and operation of SQUIDs, and the advantages of coupling them to superconducting flux transformers to improve their sensitivity to magnetic field or take spatial derivatives of the field.

Perhaps the most fascinating aspect of SQUIDs today is the remarkable diversity of their applications. Apart from a myriad of experiments in fundamental physics, the current uses of SQUIDs include chemistry—particularly nuclear magnetic resonance (NMR) and nuclear quadrupole resonance (NQR); geophysics—from surveying for natural resources to the characterization of rocks; biomagnetism—from detecting signals from the brain or heart to immunoassay; nondestructive evaluation—from locating flaws in semiconductor circuits to detecting impurities in niobium sheets for particle accelerators; and cosmology—from searching for axions or weakly interacting massive particles to detection of far-infrared and submillimeter electromagnetic radiation. Although we cannot do justice to these far-ranging fields in this short review, we discuss selected systems and applications in Section V. Section VI contains our concluding remarks.

Comprehensive reviews of SQUIDs and their applications can be found in several texts [6]–[9].

II. Theory

The superconducting pair condensate in a superconductor is described by a macroscopic wave function Ψ which has a well-defined phase ϕ. This macroscopic state is responsible for both flux quantization and Josephson tunneling, and we begin with a brief summary of the Josephson effect.

A Josephson junction consists of two weakly coupled superconducting electrodes separated—in the case of the low-T_c tunnel junction—by a thin insulating barrier. Cooper pairs tunneling through the barrier constitute a supercurrent $I = I_0 \sin\delta$, where I_0 is the critical current and δ is the difference between the phases of the order parameters in the two superconductors. For zero applied current, the two electrodes are coupled by an energy $I_0\Phi_0/2\pi$. In the absence of thermal fluctuations, the voltage V across the barrier is zero for $I < I_0$; for $I > I_0$, a voltage is developed and δ evolves with time as $\dot{\delta} = 2\pi V/\Phi_0$. At least for low-$T_c$ junctions, the *I–V* characteristics are well explained by the resistively and capacitively shunted junction (RCSJ) model. In this model, the Josephson junction is in parallel with a resistance R (which may be an external shunt) and a capacitance C. For SQUIDs, one generally needs nonhysteretic *I–V* characteristics, a requirement that is met if $\beta_c \equiv 2\pi I_0 R^2 C/\Phi_0 \leq 1$. In the limit $\beta_c \ll 1$, which is often the case for high-T_c junctions, the RCSJ model reduces to the resistively shunted junction (RSJ) model and the *I–V* characteristic in the absence of thermal noise is given by $V = R(I^2 - I_0^2)^{1/2}$ for $I \geq I_0$.

Particularly in the case of devices operating at 77 K, however, noise has an appreciable effect, and is added to the model by associating a Nyquist noise current I_N with spectral density $S_I(f) = 4k_BT/R$ with the shunt resistor. This noise term rounds the *I–V* characteristic at low voltages and reduces the apparent critical current [10]. To maintain a reasonable degree of Josephson coupling one requires the noise parameter $\Gamma \equiv 2\pi k_B T/I_0\Phi_0 = I_{\rm th}/I_0 \ll 1$; at 77 K, $I_{\rm th} \approx 3.3\ \mu$A, while at 4.2 K $I_{\rm th} \approx 0.17\ \mu$A.

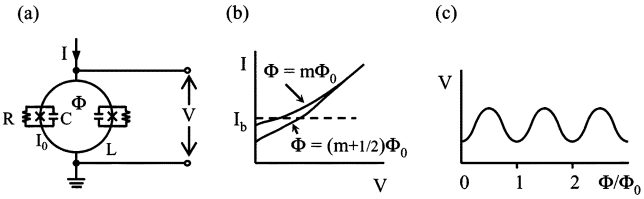

Fig. 1. DC SQUID. (a) Schematic. (b) *I–V* characteristic. (c) V versus Φ/Φ_0 at constant bias current I_b.

The dc SQUID [3] consists of two Josephson junctions connected in parallel on a superconducting loop of inductance L [Fig. 1(a)]. When the SQUID is biased with a constant current $I_b > 2I_0$ the voltage V across the SQUID oscillates with a period Φ_0 as the external magnetic flux Φ is changed [Fig. 1(b) and (c)]. To measure small changes in Φ ($\ll \Phi_0$) one generally chooses the bias current to maximize the amplitude of the voltage modulation and sets the external flux at $(2m+1)\Phi_0/4$ $(m = 0, 1, 2, \ldots)$, so that the flux-to-voltage transfer coefficient $|\partial V/\partial\Phi|_{I_b}$ is a maximum, which we denote as V_Φ. Thus, the SQUID produces a maximum output voltage signal $\delta V = V_\Phi \delta\Phi$ in response to a small flux signal $\delta\Phi$. For frequencies f well below the Josephson frequency $f_J = V/\Phi_0$, which is of the order of 10 GHz, the two independent Nyquist noise currents across the SQUID produce a white voltage noise across the SQUID with a spectral density $S_V(f)$ [11] and a white current noise around the SQUID loop with a spectral density $S_J(f)$; these two noise sources are partially correlated [12]. The intrinsic white flux noise of the SQUID is $S_\Phi(f) = S_V(f)/V_\Phi^2$; it is often convenient to introduce a noise energy per unit bandwidth $\varepsilon(f) = S_\Phi(f)/2L$. Noise imposes a second constraint on the parameters, namely, $\Phi_0^2/2L \gg 2\pi k_B T$, that places an upper limit on the value of L. We express this requirement as $\Gamma\beta_L = L/L_{\rm th} \ll 1$, where $\beta_L = 2LI_0/\Phi_0$ and $L_{\rm th} \equiv \Phi_0^2/4\pi k_B T$. At 77 K, $L_{\rm th} \approx 321$ pH and at 4.2 K $L_{\rm th} \approx 5.9$ nH.

Extensive computer simulations of dc SQUIDs [11]–[14] show that the minimum noise energy is obtained for $\beta_L \approx 1$ and that for a representative value of the noise parameter $\Gamma = 0.05, V_\Phi \approx R/L, S_V \approx 16k_B$TR, and $\varepsilon \approx 9k_B$TL$/R \approx 9k_BT\Phi_0/2I_0R$. More generally, in the limit $\Gamma\beta_L < 0.2$ one finds $\varepsilon \approx 2(1+\beta_L)\Phi_0 k_B T/I_0 R$ [14]. Thus, ε increases with temperature and, for optimized parameters, scales as $1/I_0R$. In addition to the white noise there is usually low-frequency $1/f$ noise generated by both $1/f$ noise in the critical current and by the motion of flux vortices trapped in the body of the SQUID.

The RF SQUID [4] consists of a single Josephson junction integrated into a superconducting loop that is inductively coupled to the inductance L_T of an *LC*-resonant (tank) circuit

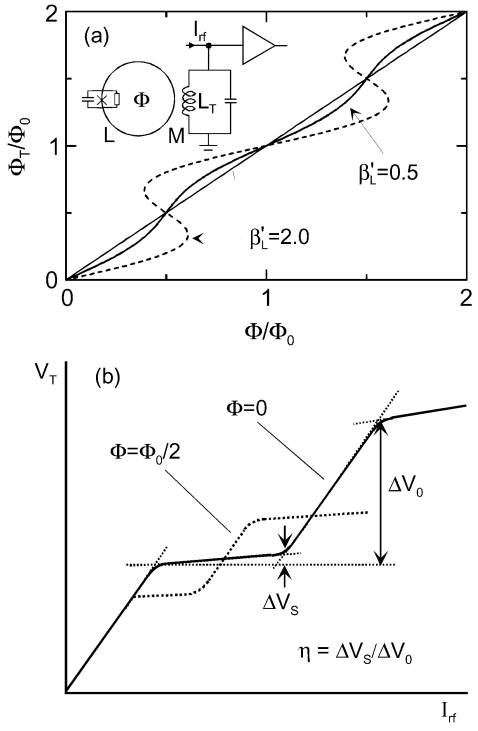

Fig. 2. RF SQUID. (a) Normalized total flux Φ_T/Φ_0 versus normalized applied flux Φ/Φ_0 for $\beta_L' = 0.5$ and 2. Inset shows RF SQUID inductively coupled to the inductor of a resonant circuit. (b) Peak RF voltage V_T across tank circuit versus peak RF current $I_{\rm RF}$ for $\Phi = 0$ (solid line) and $\Phi = \pm\Phi_0/2$. The definition of η [(2.2)] is indicated.

via a mutual inductance M [Fig. 2(a), inset]. The tank circuit is driven by an RF current $I_{\rm RF}$, and the resultant RF voltage is periodic in the flux applied to the SQUID with period Φ_0. Detailed reviews have been written by many authors, for example [13]–[17]. The total flux Φ_T in the RF SQUID is related to the applied flux Φ by $\Phi_T = \Phi - {\rm LI_0}\sin(2\pi\Phi_T/\Phi_0)$. This equation exhibits two distinct kinds of behavior [Fig. 2(a)]. For $\beta_L' \equiv 2\pi {\rm LI_0}/\Phi_0 < 1$, the slope $d\Phi_T/d\Phi = [1 + \beta_L'\cos(2\pi\Phi_T/\Phi_0]^{-1}$ is everywhere positive and the Φ_T versus Φ curve is nonhysteretic. On the other hand, for $\beta_L' > 1$, there are regions in which $d\Phi_T/d\Phi$ is positive, negative, or divergent so that the Φ_T versus Φ curve becomes hysteretic. Historically, it appears that most low-T_c RF SQUIDs were operated in the hysteretic mode, although, as we shall see, there are advantages to the nonhysteretic mode. However, the theory of noise in the nonhysteretic regime was worked out in the late 1970s, just as dc SQUIDs began to replace RF SQUIDs, and the nonhysteretic RF SQUID was not widely exploited experimentally until the advent of high-T_c SQUIDs at 77 K.

In the hysteretic mode the SQUID makes transitions between quantum states and dissipates energy at a rate that is periodic in Φ. This periodic dissipation in turn modulates the quality factor Q of the tank circuit, so that when it is driven on resonance with a current of constant amplitude the RF voltage is periodic in Φ. Fig. 2(b) shows schematically the peak voltage V_T across the tank circuit as a function of the peak RF current $I_{\rm RF}$ for $\Phi = 0, \Phi_0/2$. The characteristic consists of a flux-dependent series of "steps and risers." Theory shows that operation is optimized when $\kappa^2 Q \approx 1$, where $\kappa = M/(LL_T)^{1/2}$; under this condition

$$\rm V_\Phi \approx \omega_{RF}(QL_T/L)^{1/2} \approx \omega_{RF}(L_T/L)^{1/2}/\kappa. \qquad (2.1)$$

Note that V_Φ scales with $\omega_{\rm RF}$ and as $L^{-1/2}$.

A detailed theory has been developed for noise in the hysteretic RF SQUID operating at liquid helium temperatures (see, e.g., [13]). Thermal noise induces fluctuations in the value of flux at which transitions between flux states occur. In the case of helium-cooled RF SQUIDs in which the tank circuit voltage is detected with a room-temperature amplifier, there are also extrinsic contributions to the flux noise: the noise temperature of the RF amplifier is above the bath temperature, and a part of the coaxial line connecting the tank circuit to the amplifier is at room temperature. Representing these contributions by an effective noise temperature $T_a^{\rm eff}$, one can write the total noise energy as [15]

$$\varepsilon \approx \frac{\rm LI_0^2}{2\omega_{RF}}\left(\frac{2\pi k_B T}{I_0\Phi_0}\right)^{4/3} + \frac{2\pi\eta k_B T_a^{\rm eff}}{\omega_{RF}}. \qquad (2.2)$$

The dimensionless parameter η is defined in Fig. 2(b). This equation makes two important points. First, ε scales as $1/\omega_{\rm RF}$. Second, for low-T_c SQUIDs, the extrinsic noise energy generally dominates the intrinsic noise: for representative values $T = 4$ K, $\Gamma = 0.1, \eta = 0.2, \beta_L' = 2\pi$, and $T_a^{\rm eff} = 100$ K, we find that the extrinsic noise energy is about 20 times the intrinsic value. Thus, the overall noise energy of the hysteretic RF SQUID should not increase very much as one raises the temperature from 4 to 77 K.

For the nonhysteretic mode, $\beta_L' < 1$, the SQUID behaves as a parametric inductance, modulating the effective inductance and, hence, the resonant frequency of the tank circuit as the flux is varied. As a result, for constant drive frequency, the RF voltage is periodic in Φ. In the limit $\beta_L' \ll 1$ [18]

$$\begin{aligned}\rm V_\Phi &\approx (2/\pi)\kappa^2 Q\beta_L'\omega_{RF}L_T/M \\ &\approx (2/\pi)(\kappa^2 Q\beta_L')\omega_{RF}(L_T/L)^{1/2}/\kappa. \end{aligned} \qquad (2.3)$$

For $\Gamma \ll 1, \varepsilon \approx 3k_B TL/(\beta_L')^2 R$ for the optimized case $\beta_L' = 1$ [17]. This is generally much lower than for the hysteretic mode. When $\kappa^2 Q\beta_L' > 1$, that is, the tank circuit is strongly coupled to the SQUID, the transfer coefficient can become very high, and the noise of the preamplifier and coaxial line become relatively unimportant. The intrinsic noise energy remains low even in the large fluctuation limit $\Gamma > 1$, where the optimized value $\beta_L' = 1/\Gamma$ [19]. As a result, nonhysteretic RF SQUIDs can be operated with relatively large inductance and hence large effective area, increasing their sensitivity as magnetometers (see Section IV-C).

III. Fabrication Techniques

Modern SQUIDs are based on thin-film structures. A comprehensive overview of the fabrication of high-T_c and low-T_c thin-film devices can be found in [20] and [21] and references therein. Low-T_c SQUIDs are almost exclusively fabricated from Nb thin-films. Niobium has a transition temperature of

about 9.25 K, well above the boiling temperature of liquid helium, and is mechanically very stable; high-quality films can be fabricated by electron-beam or ion-beam evaporation or by sputtering. Tunnel junctions are patterned from Nb/AlO_x/Nb trilayers in which the AlO_x barrier is formed by oxidization of a few nanometers of Al, and the external shunt is fabricated from Mo or AuPd. The films are patterned with standard optical photolithography with linewidths down to a few micrometers. The photoresist stencil is transferred to the underlying film by "liftoff" or dry etching techniques. Niobium films can be selectively etched using reactive ion etching (RIE) with SF_6 or CF_4. The SQUID washer and spiral input coil are monolithically integrated with four or more layers. For magnetometers and gradiometers, one often forms a hybrid with a wire-wound pickup loop bonded to the thin-film input coil.

The simplicity and controllability of the Nb/AlO_x/Nb tunnel junction technology [22] surpass all earlier junction fabrication techniques. The Nb technology is mature and several hundred devices can be fabricated on a 3- or 4-in Si wafer with standard deviations of 3%–5% in I_c for junctions larger than 2 μm [21].

High-T_c SQUIDs are mostly fabricated from c axis oriented thin films of YBCO epitaxially grown on single-crystalline substrates (that is, the c axis of the perovskite-like crystal structure is normal to the substrate). These films have sufficiently strong flux pinning at 77 K to ensure both high critical current densities in the ab plane (perpendicular to the c axis) and acceptably low levels of $1/f$ noise. Low-frequency $1/f$ noise due to flux motion is rarely a problem for low-T_c thin films, but is a major issue in high-T_c films since the operating temperature (generally 77 K) is higher and pinning energies are much lower. Whereas low-T_c thin films can be deposited at or near room temperature, high-quality, c axis oriented YBCO films with the correct crystal structure require a relatively high deposition temperature, typically 700 °C–800 °C. In most cases YBCO films are deposited by pulsed laser ablation (PLD) or sputtering on single-crystalline substrates such as $SrTiO_3$. Patterning is generally carried out with standard photolithography and Ar ion beam etching. Sometimes, especially for larger structures, chemical wet etching is used.

In contrast to low-T_c superconductors, there is no trilayer junction technology; of the many types of high-T_c Josephson junctions developed over the last 15 years, only a few are suitable for SQUIDs. Grain boundary bicrystal junctions [23], that is, a microbridge patterned across the grain boundary of a film grown on a bicrystal substrate, have been most widely used to fabricate high-T_c SQUIDs. Other junction types which are sometimes used include grain-boundary step-edge, superconductor-normal metal-superconductor step-edge and quasi-planar ramp-type junctions. In contrast to Nb/AlO_x/Nb junctions the standard deviations of the junction parameters are relatively high: 20%–30% in the best case for bicrystal junctions [20], [21]. Given the high price of bicrystal substrates and that the junctions can be positioned only across the grain boundary, ramp-type junctions probably represent the future of high-T_c SQUID technology; however, further improvements in the technology will be necessary.

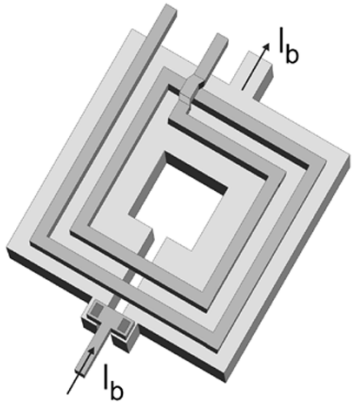

Fig. 3. Schematic of low-T_c dc SQUID with integrated input coil. The two Josephson junctions are at bottom left and are biased with a current I_b.

The fabrication of complete SQUID structures from single YBCO thin films is relatively well controlled. The yield is largely determined by the film quality and the spread of junction parameters. On the other hand, although very successful prototype SQUID devices involving multilayers have been demonstrated, this technology is not mature. In these structures, each layer has to be patterned separately and devices with input coils or multiloops all contain crossovers and vias. The crucial requirement is that the upper YBCO film has to grow on the patterned underlying layers and across patterned edges with high crystalline perfection; details are discussed in [20] and [24]–[26]. Although in the mid-1990s a few groups demonstrated that high-quality multilayer SQUID magnetometers can be fabricated with excellent noise performance [27]–[29]; subsequently, most high-T_c SQUID magnetometers have been single-layer.

In contrast to low-T_c technology, high-T_c SQUID magnetometers are mostly fabricated one at a time. This is mainly because substrates such as $SrTiO_3$ are both expensive and not available in sizes greater than 1 in. A major concern is that YBCO deteriorates in the presence of water; thus, high-T_c devices require a passivation layer or hermetically sealed encapsulation.

IV. Design, Operation, and Performance

A. Low-T_c DC SQUIDs

Virtually all low-T_c dc SQUIDs used today involve Nb-AlO_x-Nb Josephson junction technology [22] and a thin-film Nb planar square washer (Fig. 3). A Nb multiturn input coil deposited over the washer, with an intervening insulating layer, provides efficient inductive coupling to the SQUID loop [30]. A variety of different input circuits can be coupled to this coil, for example, to produce voltmeters, amplifiers, magnetometers, or gradiometers [7], [9]. The input circuit converts the physical quantity to be measured into magnetic flux which is sensed by the SQUID, producing an output voltage.

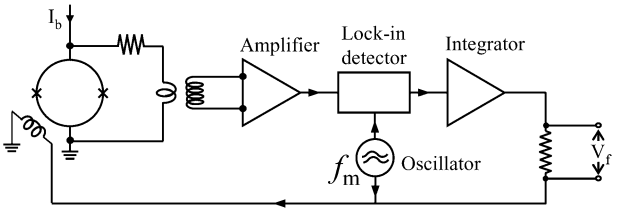

Fig. 4. FLL for operation of a dc SQUID.

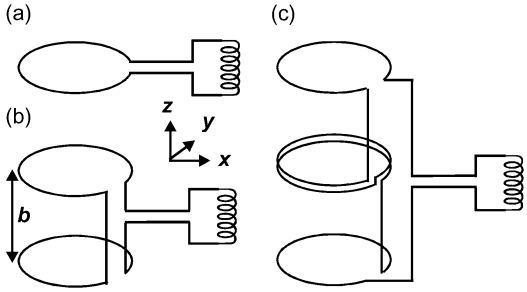

Fig. 5. Superconducting, wire-wound flux transformers. (a) Magnetometer. (b) First-derivative, axial gradiometer. (c) Second-derivative, axial gradiometer.

The design criteria for dc SQUIDs are based on the constraints $\beta_c \lesssim 1$ and $\beta_L \approx 1$ (Section II). Numerical simulations predict that the optimal noise energy scales as $T(LC)^{1/2}$, so that the SQUID inductance L and the junction capacitance C should be made as small as possible. In practice, the lower limit of C is determined by the junction technology (typically 0.5–1 pF for Nb junctions), and $L = 1.25\ \mu_0 d$ cannot be made much smaller than 10 pH; here d is the dimension of the hole in the washer of outer dimension D. Typically, values of L range from 10 pH to a few hundred pH, the larger values being required to achieve reasonably efficient coupling to most practical input circuits. For a given value of L, one chooses I_0 to satisfy $\beta_L \approx 1$ and R to achieve $\beta_c \lesssim 1$. The number of turns n on the input coil ranges from about 4 to 50; for a 100–pH SQUID, the coil inductance $L_i \approx n^2 L$ correspondingly ranges from about 1.6 to 250 nH, and the mutual inductance $M_i \approx nL$ from 0.4 to 5 nH. In practice, there are parasitic resonances that can induce deleterious structure on the *I–V* and V-Φ characteristics when the resonant frequency corresponds to the Josephson frequency or a multiple of it. These resonances require resistive damping [31], [32].

In most applications, the signal from the SQUID is amplified and fed back either as a current to the input circuit or as a flux to the SQUID loop. Feedback linearizes the SQUID response, enabling one to detect minute fractions of a flux quantum as well as to track many flux quanta [33]. A widely used flux-locked loop (FLL) involves flux modulation of the SQUID with a peak-to-peak amplitude of $\Phi_0/2$ and a frequency f_m of 0.1–10 MHz (Fig. 4). The resulting oscillating voltage across the SQUID is coupled via a resonant matching circuit or transformer to a room-temperature preamplifier and then lock-in detected at frequency f_m. After integration, the resulting signal is fed back as a current through a resistor to a coil, thus keeping the flux in the SQUID constant at an optimum working point on the V-Φ characteristic. This flux modulation scheme greatly reduces $1/f$ noise from in-phase fluctuations of the critical currents in the junctions. Low-frequency $1/f$ noise from out-of-phase critical current fluctuations can be eliminated by an additional bias current reversal scheme [34]. An alternative FLL involves "direct readout," which eliminates the need for a coupling network between the SQUID and amplifier. This scheme enables one to use particularly simple electronics, can be combined with a bias reversal scheme if necessary, and can have an FLL bandwidth up to about 10 MHz [33].

A typical dc SQUID at 4.2 K exhibits a flux noise of about $10^{-6}\Phi_0\ \mathrm{Hz}^{-1/2}$, corresponding to a noise energy of the order of $10^{-32}\ \mathrm{JHz}^{-1}$, at frequencies down to about 1 Hz. The bandwidth of the FLL varies widely, from 50 kHz up to 10 MHz, while the slew rate may be as high as $10^7\Phi_0 s^{-1}$ [33].

The most widely used input circuits are superconducting flux transformers configured as magnetometers or spatial gradiometers (Fig. 5). For a magnetometer [Fig. 5(a)], the input coil is connected to a much larger superconducting pickup loop of inductance L_p and area A_p. The pickup loop may be a Nb wire or a thin film of Nb integrated with the SQUID on a single chip [32]. The transformer greatly increases the field capture area A_{eff} above that of the bare SQUID, Dd. Within some approximations, for a given value of L_p, one finds that A_{eff} is a maximum when $L_i = L_p$; one can achieve this condition by choosing n appropriately [32]. The magnetic field noise referred to the pickup loop $S_B^{1/2}(f)$ is related to the flux noise of the SQUID by $S_B^{1/2}(f) = S_\Phi^{1/2}(f)/A_{\mathrm{eff}}$. For example, a thin-film magnetometer with an $8 \times 8\ \mathrm{mm}^2$ pickup loop and a SQUID inductance of about 200 pH achieved a magnetic field noise close to $1\ \mathrm{fT} \cdot \mathrm{Hz}^{-1/2}$ at frequencies down to 1 Hz [35].

An alternative approach to high magnetic field sensitivity is the multiloop magnetometer or fractional turn SQUID [36]. Connecting N loops in parallel reduces the total inductance while keeping A_{eff} large. Drung *et al.* developed a Nb thin-film version of the multiloop dc SQUID resembling a cartwheel with N spokes [37]. At 4.2 K, a 7-mm-diameter device with $N = 8$ and $L = 420$ pH achieved a noise of $0.9\ \mathrm{fT} \cdot \mathrm{Hz}^{-1/2}$ at frequencies down to 2 Hz [38].

Spatial gradiometers [Fig. 5(b) and (c)] are required for SQUID detection of weak signals against a background of magnetic noise many orders of magnitude higher. An excellent example is detecting signals from the brain (Section V-A), for which the SQUID system and the subject are placed inside a magnetically shielded room (MSR). However, most MSRs do not offer sufficient attenuation, in particular, of 50- or 60-Hz fields, and one requires a gradiometer to discriminate against distant noise sources with small gradients in favor of nearby signal sources. The traditional first-derivative, low-T_c gradiometer [Fig. 5(b)] is wound from Nb wire: two pickup loops wound in opposition with a separation b of typically 0.1 m are connected in series with the input coil of a SQUID. With ideally balanced input coils, a uniform axial field B_z couples zero

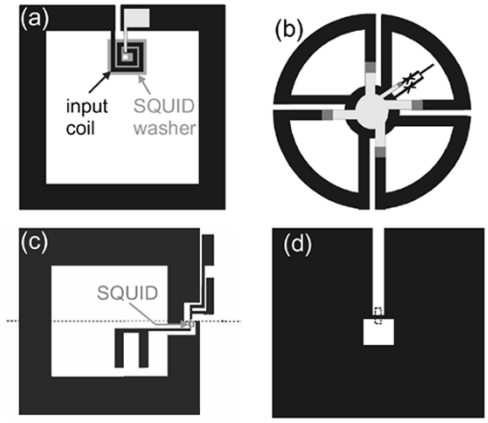

Fig. 6. High-T_c magnetometers. (a) DC SQUID inductively coupled to a multiturn input coil connected to a pickup loop. (b) Multiloop dc SQUID magnetometer. (c) Single-layer, directly coupled magnetometer, dashed line indicates bicrystal grain boundary. (d) Large area RF SQUID; dashed line indicates step-edge grain boundary.

net flux into the SQUID, while a gradient $\partial B_z/\partial z$ couples a proportionate flux. In practice, asymmetries in the coil windings and parasitic inductances result in a response to a uniform field. The ratio of this response to that of uniform field applied to one of the pickup loops is defined as the gradiometer balance, which is typically 10^{-3} to 10^{-2}. Fig. 5(c) shows a second-order gradiometer, which measures $\partial^2 B_z/\partial z^2$. Planar gradiometers with thin-film pickup loops measure off-diagonal gradients, such as $\partial B_z/\partial x$ or $\partial^2 B_z/\partial x \partial y$. Alternatively, one can subtract the outputs of two first-derivative gradiometers electronically or in software to form second- or even third-order gradiometers; in addition, subtracting the outputs from three orthogonal magnetometers produces a high degree of balance for the first derivative [9], [14], [39].

B. High-T_c DC SQUIDs

Achieving optimized high-T_c dc SQUIDs for operation at 77 K is considerably more difficult than for low-T_c dc SQUIDs: first, there is no mature high-T_c Josephson junction technology, and second, raising the temperature to 77 K has a drastic impact on the thermal noise. To achieve the small thermal fluctuation limit at 77 K, I_0 has to be well above 3 μA and L well below 100 pH (Section II). Both requirements can easily be met for uncoupled dc SQUIDs, enabling, for example, a white flux noise of 1.5 $\mu\Phi_0$ Hz$^{-1/2}$ and a corresponding noise energy of 2×10^{-32} J/Hz to be achieved at 77 K for a YBCO dc SQUID with $L \approx 30$ pH [40]. However, efficient coupling to a flux transformer generally requires significantly larger inductances, so that one has to compromise between degraded white flux noise and inefficient coupling of the input circuit. Furthermore, $1/f$ noise is usually much higher in high-T_c SQUIDs than in their low-T_c counterparts.

There are two general approaches to making sensitive high-T_c magnetometers: multilayer structures and single-layer devices. Most multilayer magnetometers consist of a pickup loop connected to a multiturn input coil that is inductively coupled to a washer SQUID [Fig. 6(a)]. This may be achieved by fabricating the SQUID and flux transformer on separate substrates which are subsequently pressed together face-to-face in a flip-chip configuration, or by integrating the input coil with the SQUID. The flip-chip approach enables one to choose the highest performing SQUID from a batch. The lowest levels of white noise achieved at 77 K and 1 kHz with the two approaches are comparable: 8.5 fT $\cdot$ Hz$^{-1/2}$ ($A_p = 9 \times 9$ mm^2) [27] and 6 fT $\cdot$ Hz$^{-1/2}$ ($A_p = 16 \times 16$ mm^2) [29] with flip-chip devices, and 9.7 fT $\cdot$ Hz$^{-1/2}$ for a flux transformer ($n = 10.5, A_p = 8.3 \times 8.6$ mm^2) integrated with a 130-pH SQUID [41]. Unfortunately, high-T_c multilayer flux transformers typically produce excess low-frequency noise [14], so that with typical $1/f$ noise corner frequencies of 10–1000 Hz, the magnetic field noise at 1 Hz tends to be much higher. Multiloop high-T_c magnetometers have also been fabricated [Fig. 6(b)]. At 77 K, a 7-mm-diameter device with $N = 16$ and $L = 145$ pH achieved a white noise of 18 fT $\cdot$ Hz$^{-1/2}$, and 37 fT $\cdot$ Hz$^{-1/2}$ at 1 Hz [28].

The single-layer device—the so-called directly coupled magnetometer [Fig. 6(c)]—is much more straightforward to fabricate than multilayer devices, and exhibits lower levels of $1/f$ noise. The pickup loop injects current directly into the SQUID loop. Despite the substantial inductance mismatch ($L_p \gg L$), A_{eff} is significantly enhanced resulting in a low magnetic field noise down to frequencies of about 1 Hz [42]. Making the pickup loop with a large linewidth reduces the mismatch [43]. With such an improved design, a white noise of 24 fT $\cdot$ Hz$^{-1/2}$ was achieved with a 10×10 mm^2 pickup loop and $L = 100$ pH [44].

C. RF SQUIDs

RF SQUIDs made from conventional superconductors, operated at 4.2 K at a typical frequency of 20 MHz with the resonant circuit connected to a room-temperature preamplifier, were used in various applications in the 1970s until they were gradually replaced by Nb dc SQUIDs in the 1980s. As with dc SQUIDs, they were almost invariably operated in an FLL. The *system* flux noise of these early RF SQUIDs, which were almost always operated in the hysteretic mode, was generally dominated by extrinsic noise sources (Section II). These noise sources are drastically reduced by operating the SQUID at 1 GHz or higher, which both increases the available signal and decreases the intrinsic noise, and by cooling the semiconductor preamplifier [45], [46]. Today, planar, thin-film Nb RF SQUIDs at 4.2 K achieve a noise energy comparable to that of the dc SQUIDs [45]–[47]. However, because of the relatively complex infrastructure required for RF SQUIDs, they are rarely used at liquid helium temperatures.

On the other hand, the situation at 77 K is rather different. As the temperature is increased from 4.2 to 77 K, the intrinsic noise of both RF and dc SQUIDs increases, but in the former case the noise contributions of the preamplifier and the line coupling it to the tank circuit do not increase. Consequently, one may operate a high-T_c RF SQUID at 77 K and (say) 1 GHz with a room-temperature preamplifier with little degradation in performance compared with a similar device

at 4.2 K with the same preamplifier. Furthermore, it turns out that the inductance of nonhysteretic RF SQUIDs can be made larger than that of the dc SQUID before the performance begins to deteriorate due to thermal fluctuations [19], [48], [49]. Consequently, they can have inductances up to several 100 pH, and correspondingly large effective areas, $\approx Dd$. For example, at 77 K, a magnetic field noise of 100 fT $\cdot$ Hz$^{-1/2}$ was achieved using a washer with 10×10 mm^2 outer dimensions [Fig. 6(d)] and an inductance of 300 pH, coupled to a conventional tank circuit operating at 150 MHz [50]. Subsequently, large washer RF SQUIDs or the combination of smaller washer SQUIDs with large washer-type flux concentrators have been operated at about 1 GHz using coplanar resonators or bulk high-Q dielectric resonators as microwave tank circuits [46], [47]. These devices are generally operated in the nonhysteretic mode. The developments have resulted in a magnetic field noise of 20–30 fT $\cdot$ Hz$^{-1/2}$, albeit increasing below about 100 Hz [51].

The sensitivity of a high-T_c RF SQUID was further improved by means of a planar flux transformer with a multiturn input coil [52]. The flux transformer (with a 10×10-mm^2 pickup loop connected to the input coil) and a planar resonator containing a single-turn RF input coil were integrated on one chip that was inductively coupled to the two-hole SQUID on a second chip. The multiturn input coil couples low-frequency signals to one SQUID loop, while the RF input coil couples the resonator to the other loop. At 77 K, the lowest magnetic field noise achieved was 12 fT $\cdot$ Hz$^{-1/2}$ above 1 kHz [52]; the noise increased strongly at lower frequencies, probably due to vortex motion.

D. Low-Frequency $1/f$ Noise

Since many applications of SQUIDs require low noise at low frequencies, $1/f$ noise from critical current fluctuations and vortex motion in thin-film structures is an important issue. Particularly for high-T_c SQUIDs, $1/f$ noise is a severe problem because I_0-fluctuations in high-T_c junctions are several orders of magnitude larger than for Nb tunnel junctions [14]. Consequently, high-T_c dc SQUIDs must be operated with a bias-reversal scheme. In the case of the RF SQUID, the combination of the RF bias and flux modulation greatly reduces this source of noise [53]. More importantly, low-frequency noise due to the thermally activated hopping of vortices still limits the performance of many practical high-T_c SQUIDs. This problem is exacerbated for devices cooled in the earth's magnetic field. The magnitude of the low-frequency flux noise is inversely correlated with the quality of the high-T_c films, which in turn is determined by a variety of defects. However, a detailed understanding of the interplay between microstructure and noise properties of high-T_c thin films is still lacking. Furthermore, the geometry of the devices and the patterning process significantly affect both the noise, since the contribution of fluctuating vortices to the flux noise depends strongly on their position and on the device geometry, and the conditions for vortex entry. The introduction of narrow linewidths [54] and flux dams [55] significantly reduces low-frequency noise in high-T_c SQUIDs, by preventing vortex entry into the films. It appears that these approaches are more successful than attempts to improve flux pinning in the films.

Fig. 7. System for MEG with 275 sensor channels and 29 reference channels (courtesy CTF Systems, Inc.).

V. Applications

We first briefly discuss several commercially available systems that illustrate various applications, and then describe three widely different applications under development today: biosensors, high-frequency amplifiers, and magnetic resonance imaging (MRI). Elsewhere in this special issue, Zmuidzinas and Richards [56] describe the use of SQUIDs to read out superconducting sensors for millimeter-wave detectors.

A. Commercial Systems

Most SQUIDs ever made are incorporated into whole-head systems for magnetoencephalography (MEG)—the detection of magnetic fields produced by the brain [39], [57]. These systems are manufactured by at least four companies, CTF, Neuromag, 4-D NeuroImaging, and Yokagawa; an example is shown in Fig. 7. A typical helmet contains about 300 sensors, including a number of reference sensors for noise cancellation, cooled to 4.2 K. The sensors are generally configured as first-order gradiometers, measuring either an axial gradient, or sometimes an off-diagonal gradient, such as $\partial B_z/\partial x$. The magnetic field sensitivity referred to one pickup loop is typically 3–5 fT $\cdot$ Hz$^{-1/2}$. Each SQUID is operated in its own FLL, and the outputs from all the channels are recorded digitally for subsequent analysis.

The biggest single challenge is the suppression of environmental magnetic noise. For example, a typical signal from the brain might be 50 fT, while urban noise may vary from 10 nT -1 μT rms. Thus, to obtain a good signal-to-noise

ratio, a noise rejection of 10^8 (160 dB) is required. This is achieved in part by the use of gradiometers, which reject distant noise sources in favor of nearby signal sources. Signals from two first-order gradiometers can be subtracted in software to form a second derivative. However, because the hardware gradiometers do not reject uniform magnetic fields precisely, it is necessary to add further corrections from a three-axis reference magnetometer. The signals from more devices can be combined in software to form a third derivative. Whereas the field from a magnetic dipole falls off with distance r as $1/r^3$, the first, second, and third derivatives fall off as $1/r^4, 1/r^5$, and $1/r^6$, respectively; thus, the third-order gradiometer, in particular, strongly attenuates distance noise sources. Nonetheless, most systems are surrounded by an MSR made of a high-permeability material that further reduces ambient fluctuations in magnetic field.

Whole-head systems are in use in numerous hospitals in the United States, Europe, and Japan, primarily for mapping of the brain prior to surgery. When the brain is stimulated, by auditory, somatosensory, or visual means, a small region of the cortex responds by producing magnetic signals that are recorded by the array of SQUIDs surrounding the patient's head. Each signal source can be modeled approximately as an equivalent current dipole, that is, as a tiny battery embedded in the conducting medium of the brain. By solving the inverse problem one can locate the source of a given dipole, typically to within about 2 mm. The most widely used application is presurgical mapping of brain tumors. Although a brain tumor can be located precisely by MRI, this image does not reveal the function of the surrounding brain tissue, which may be severely displaced by the tumor. MEG is used to map the function of the brain in the vicinity of the tumor, enabling the subsequent surgery to be performed via the least invasive path. This procedure has dramatically improved the outcome of brain tumor surgery.

A second important application is to patients suffering from focal epilepsy. The MEG system detects the magnetic signals generated by spontaneous interictal discharges in the epileptic source. In many cases, these sources can be modeled as equivalent current dipoles and can, thus, be localized. If surgery is appropriate, it is again guided by mapping the function of the surrounding tissue. More recently, these mapping techniques have been used to determine the severity of brain trauma, for example, following a blow to the head or a stroke, and to monitor the neurological recovery. Several other applications of MEG are being explored, including language mapping and studies of patients suffering from schizophrenia or from Alzheimer's or Parkinson's disease.

A related medical application is magnetocardiography (MCG). A number of companies have developed MCG systems at one time or another, including CTF, 4D-Neuro-Imaging, Hitachi, Neuromag, Philips, and Siemens. Recently, CardioMag Imaging and SQUID International (formerly SQUID-AG) have marketed systems specifically intended to be operated without magnetic shielding.

In MCG, an array of SQUID gradiometers—anywhere from 9 to 64—is placed just above the chest of the reclining subject to record the magnetic fields produced by the heart. From these "magnetocardiograms," one reconstructs the current flow in the heart, which varies greatly during the cardiac cycle. There is a considerable body of research [58], [59] on both the fundamental processes which produce the magnetic signals and the diagnostic potential of MCG. One application is the localization of accessory pathways—essentially electrical short circuits—that are a source of heart arrhythmia. Another is the diagnosis of ischemia—oxygen starvation of the heart muscle due to narrowed arteries—which can severely distort the magnetic dipole pattern characteristic of the healthy heart during the repolarization cycle. A third potential application—in hospital emergency rooms—is the rapid diagnosis of a suspected heart attack. Yet another extensively studied application is fetal MCG. Clinical studies have been undertaken of these and other modalities over the past decade and continue today. The general conclusion appears to be that the diagnostic ability of MCG is superior to that of electrocardiography (ECG) in at least some applications. However, the high cost of MCG compared to ECG has proven to be a significant barrier, and MCG is not yet adopted clinically. This reluctance may be due, in part, to the fact that the systems marketed so far have not incorporated cryocoolers and, thus, require regular transfers of liquid helium. This is an application for which high-T_c SQUID gradiometers have sufficiently low noise, and the introduction of a cryocooled high-T_c system might well result in a much more widespread use of this technique.

The most widely distributed commercial SQUID system is Quantum Design's Magnetic Property Measurement System (MPMS). The essential feature is the use of a gradiometer to measure the magnetic properties of a sample inserted into one of its pickup loops via a vertical tube with room-temperature access. The temperature of the sample can be varied from about 2 to 400 K, and the magnetic field can be varied from zero to ± 7 T. The system can be used to measure both the intrinsic magnetic moment of a sample in zero magnetic field and the magnetic susceptibility by applying a magnetic field. The original system operated in liquid helium, but a version equipped with a cryocooler is now available: the latter is an excellent example of a turnkey system where the operator does not need to be aware that it contains a superconducting device. The MPMS has found a great variety of applications in physics, materials science, geology, electronics, and biology. Examples of its applications include high-T_c and heavy fermion superconductors, antiferromagnets, fullerenes, spin glasses, magnetic–optic materials, nanocomposites, amorphous alloys, ceramics, metalloproteins, sea-bed lava, and iron concentrations in chlorophyll.

A somewhat related but more specialized instrument which has also sold widely is the Superconducting Rock Magnetometer manufactured by 2G Enterprises (Fig. 8). The magnetometer has a horizontal room-temperature access and is aimed specifically at determining the magnetic moment—along three axes—of rock core samples up to 0.12 m in diameter and 1.5 m in length. The magnetic moment noise of the system is 10^{-12} Am^2. With the aid of cryocooled thermal radiation shields, the system can run for

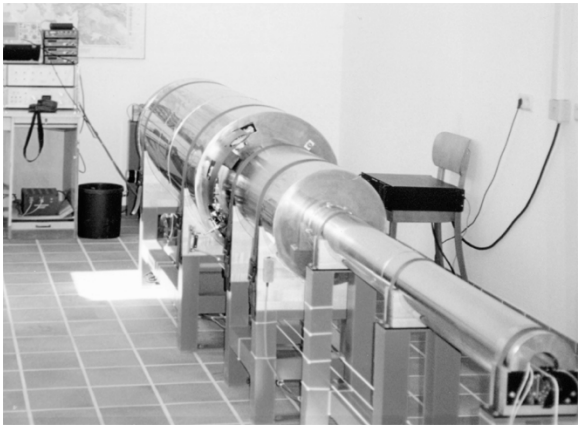

Fig. 8. Rockmagnetometer (courtesy 2G Enterprises).

a remarkable 1000 days between liquid helium refills. Thus, the need for cryogenics is virtually invisible to the user, and this instrument has become the standard rock magnetometer of the geophysics community. One application is to measure the magnetic moment of sedimentary cores taken from the ocean basins to study the polarity reversal of the earth's field over geologic time.

The above examples involve low-T_c SQUIDs. Neocera's Magma involves a high-T_c SQUID, and is used to image currents in semiconductor packages. The SQUID—which is cooled by a cryocooler—is mounted just above a thin window at the bottom of the vacuum enclosure. The package is scanned in a two-dimensional (2-D) raster below the window and the low-frequency oscillating current applied to the part of the circuit in question produces a magnetic field that is detected by the SQUID. An inversion algorithm produces an image of the current paths and even provides depth resolution. This instrument is used to locate faults in packages, for example, open lines, unintended shorts between metallic layers, and wire bond failures. A useful function is the ability to store the image of a functioning package from which the image of a defective package can be subtracted, thus giving a rapid diagnosis of the failure.

There are a number of other—generally small—companies that market custum-made systems or devices. For example, Tristan produces a liver susceptometer for determining the ion content of the liver, a system for gastromagnetism, and an instrument to map the cardiac currents in rabbit hearts; Easy SQUID markets systems for nondestructive evaluation of defects in materials. Several companies—including Easy SQUID, Hypres, Jülich SQUID AG, Magnicon, Quantum Design, Seiko, Star Cryoelectronics, Supracon, and Tristan market SQUIDs and, in some cases, readout electronics.

B. Biosensors

Several groups have developed biosensors in which a SQUID detects the presence of antigens selectively labeled with magnetic markers [60]–[65]. The superparamagnetic particles, which are commercially available and usually 20–100 nm in diameter, typically consist of a cluster of γ-Fe_2O_3 subparticles each $\sim$10 nm in diameter. When a magnetic field is applied to immobilized particles, they become magnetized; when the field is removed, the magnetization relaxes via Néel relaxation in a time which depends exponentially on the volume of an individual subparticle, and is typically 1 ms to 1 s. On the other hand, if the particle is freely suspended in a liquid, the application of the magnetic field aligns the particle; removal of the field enables the particle to undergo Brownian relaxation, causing the magnetic moment of an ensemble of particles to decay in a time that is typically tens of microseconds. The distinction between fast Brownian rotation and slow Néel relaxation enables one to distinguish free and immobilized particles.

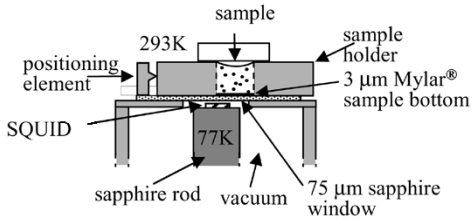

Fig. 9. Top portion of SQUID microscope. The SQUID is mounted on a sapphire rod thermally connected to a liquid nitrogen reservoir (not shown). A 75-μm-thick sapphire window separates the vacuum enclosure from the atmosphere. (From [63], with permission.)

In an assay, the magnetic particles are attached to the antibody appropriate to the particular antigen being sought. When suspensions of the antibodies and antigens are mixed together, the antibodies attach to the antigens, thereby labeling them magnetically. On the other hand, if the antibody encounters a different antigen, the possibility of binding is low, so that the assay is specific to a chosen target.

There are various approaches to magnetic assaying. One of them involves immobilizing the magnetically tagged antibodies on a substrate and scanning the substrate close to a SQUID in the presence of a magnetic field parallel to the direction of motion [64]. The amplitude of the magnetic field detected by the SQUID is a measure of the total magnetic moment of the sample and, hence, of the number of antigens. This procedure requires one to remove the unbound particles from the substrate with a wash step. A second approach involves measuring the relaxation of the magnetic particles [60]–[63]. This procedure can be performed in two ways: the target antigens may be attached to a substrate or they may be freely suspended. We briefly describe an experiment based on the second method involving a high-T_c SQUID "microscope."

The microscope [63] (Fig. 9) brings a sample at room temperature and atmospheric pressure within 100–200 μm of a high-T_c SQUID, which is at 77 K in a vacuum. The SQUID is mounted on a sapphire rod, which is cooled by a reservoir of liquid nitrogen. The 20-μL liquid sample is contained in a nonmagnetic holder with a 3-μm-thick bottom, offset laterally from the center of the SQUID to maximize the flux coupling. The measurement involves pulsing a 0.4 mT field parallel to the SQUID on for 1 s and off for 1 s, and recording the magnetic decay while the field is off. Data from 100 pulses are averaged.

In one set of experiments [63], the target bacteria were the (nonvirulent) DP-L2161 strain of *Listeria monocylogenes*.

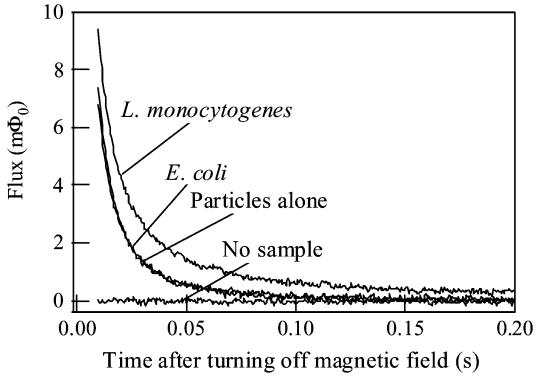

Fig. 10. Magnetic decay signals, averaged 100 times. (From [63], with permission.)

The magnetic particles were coupled to polyclonal goat anti-*Listeria* IgG antibodies. The bacteria and antibodies were incubated, and a 20-μL sample was transferred to the sample holder. A typical flux decay trace, labeled *L-monocytogenes* in Fig. 10, can be fitted to [61]

$$\Phi(\mathrm{t}) = \Phi_{\mathrm{s}} \ln(1 + \tau_{\mathrm{mag}}/\mathrm{t}) + \Phi_{\exp}(-\mathrm{t}/\tau_{\exp}). \qquad (5.1)$$

The logarithmic decay arises from the wide distribution of superparamagnetic particle sizes [65]. In this magnetic relaxation process, the relatively large listeria cell ($\sim$1 μm) rotates slowly, so that the observed signal is predominantly from the Néel relaxation. The flux amplitude Φ_s is proportional to the number of magnetic particles undergoing Néel relaxation, and $\tau_{\mathrm{mag}} = 1$ s is the magnetization time. The second exponential term in (5.1) arises from particle aggregates, which are large enough to undergo Brownian relaxation on a measurable timescale without being bound to targets. Fig. 10 also shows the decay curves obtained when *L. monocytogenes* was replaced with *E. coli*. Both curves were obtained in the presence of unbound, labeled antibodies, for which the Brownian rotation was too rapid to be detected by the SQUID. Finally, we see from Fig. 10 that the empty sample holder produces no detectable signal. The limit of detection was estimated to be about 10^5 *L. monocytogenes* in the 20-μL sample volume. This sensitivity could be considerably improved by matching the area of the sample more effectively to the effective area of the SQUID, while reducing the height of the column of liquid.

A major advantage of magnetic labeling is that the relaxation measurements distinguish between bound and unbound antibodies, thus avoiding the need to wash away unbound labels as is the case in most immunoassay techniques. The measurement system could be adapted to scan a plate containing (say) 96 wells, as is commonly used in immunoassay. The high sensitivity and high throughput that are potentially achievable make this technique worthy of further study for practical application, for example, for immunoassay and as a detector of pathogens in the environment.

C. Microstrip SQUID Amplifier

The vast majority of SQUIDs are used at frequencies below 1 kHz; some are used, open loop, at frequencies up to about 100 MHz [66]. However, there has been interest in developing SQUIDs for frequencies of the order of 1 GHz, both as an intermediate frequency amplifier to follow a superconductor–insulator–superconductor mixer [56] for radio astronomy and as a preamplifier for an axion detector [67]. The difficulty in extending the frequency range of the square washer SQUID (Section IV-A) is the rolloff in gain produced by parasitic capacitance between the input coil and the washer. One way to circumvent this problem is to place the input coil inside the hole in the SQUID washer [68]. In a different approach, Mück *et al.* [69]–[72] applied the signal between one end of the input coil and the SQUID washer, making use of the fact that these form a microstrip. We briefly describe this "microstrip SQUID amplifier."

The microstrip SQUID amplifier consists of a square washer SQUID, with the signal applied between one end of the input coil and the washer via a cold attenuator that matches the input to the 50-Ω output of a signal generator. The SQUID is flux- and current-biased to maximize V_Φ. The voltage across the SQUID is coupled via a cold matching network to a low-noise, room-temperature amplifier. As a function of frequency, the amplifier shows a peak in the gain that may vary from 0.2 to 4 GHz, depending on the number of turns on the input coil, its length ℓ, and the SQUID inductance L. At first sight, one might assume that the peak occurs at the fundamental resonance of the microstrip, that is, when ℓ is equal to a half-wavelength. In fact, this is not the case; the calculation of the frequency at which the peak occurs is complicated by the inductance n^2L coupled in from the SQUID (Section IV-A), and by feedback from the SQUID output to the microstrip via its self-capacitance.

At frequencies up to 1 GHz, the gain is typically 20 dB and the noise temperature T_N somewhat below 1 K for a bath temperature of 4.2 K. The noise temperature scales with the bath temperature T in this temperature range; for $T = 1.8$ K, a noise temperature of about 0.2 K was achieved at 365 MHz, using a cooled semiconductor postamplifier [71]. This noise temperature is an order of magnitude lower than that of a cooled high-electron mobility transistor (HEMT). However, much lower noise temperatures are achievable at dilution refrigerator temperatures. Mück *et al.* [72] constructed an amplifier in which two SQUIDs were connected in series and followed by a cooled semiconductor postamplifier. The input to the first stage was coupled to an *LC* circuit with a resonant frequency of $f_0 = 519$ MHz, which provided a Nyquist noise source. Measurements of the noise at the output of the amplifier chain as a function of the frequency yielded the noise temperature of the input SQUID amplifier, which is plotted versus bath temperature in Fig. 11. Down to about 200 mK, T_N scales linearly with T, flattening out at about 50 mK—a factor of two above the quantum-limited noise temperature $T_Q = hf_0/k_B \approx 25$ mK. The flattening of T_N at low temperatures was ascribed to hot electrons in the resistive shunts of the SQUID.

At low operating temperatures and frequencies around 0.5 GHz, the microstrip SQUID amplifier has a substantially lower noise temperature than any other device. The operating frequency may be tuned over a factor of about two by connecting a varactor diode across the otherwise open end

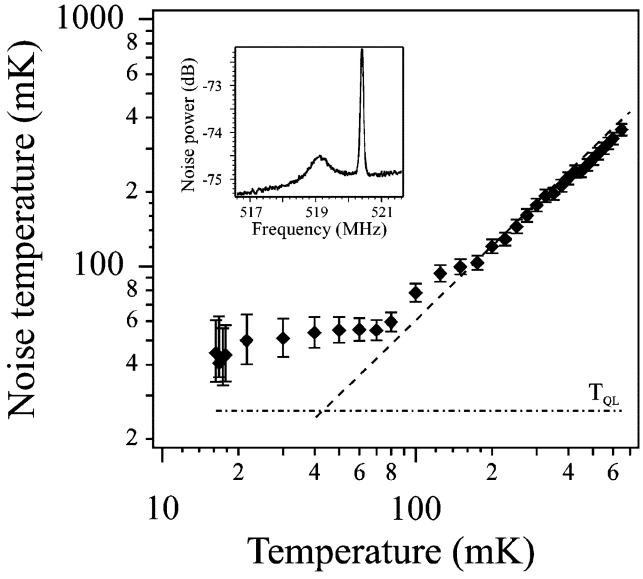

Fig. 11. Noise temperature of microstrip SQUID at 519 MHz versus temperature. The dashed line through the data corresponds to $T_N \propto T$, and the dot-dashed line indicates $T_Q = hf/k_B \approx 25$ mK. Inset is noise peak produced by *LC*-tuned circuit at 20 mK; peak at 520.4 MHz is a calibrating signal. (From [72], with permission.)

of the microstrip [70]. In addition to its potential application to axion detectors [67], the amplifier is being used as a postamplifier for the RF single-electron transistor (RFSET) [73], potentially enabling it to attain quantum-limited charge detection.

D. Microtesla NMR and MRI

NMR [74] is widely used to investigate the structure of materials at frequencies that range up to 900 MHz, corresponding to a magnetic field for protons of about 21 T. The NMR frequency is a direct measure of the local magnetic field experienced by a given nucleus, providing an exquisite tool to measure magnetic interactions. In MRI [75], the application of magnetic field gradients enables one to image the human body noninvasively, typically at 1.5 T. In view of the importance of these techniques, it is hardly surprising that the high sensitivity of SQUIDs has been widely exploited for NMR. In his review, Greenberg [76] lists some 100 different SQUID-based experiments on gases, liquids and solids at nuclear temperatures that range from 300 K to below 1 μK. Recently, promising advances have been made in low-field NMR and MRI [77]–[85], which we briefly describe.

Many nuclei have a magnetic moment $\vec{\mu} = \gamma\hbar\vec{I}$, where $\vec{I}$ is the nuclear angular momentum in units of $\hbar$ and γ is the gyromagnetic ratio. For protons, with spin $1/2$, the projection of $\vec{I}$ on the z axis, I_z, is $\pm 1/2$. In a magnetic field B_0 along the z axis, the potential energy of the nucleus $-\vec{\mu}\cdot\vec{B}_0$ takes one of the corresponding values $-\mu_z B_0 = \pm\gamma\hbar B_0/2$. The two energy levels are, thus, split by $\hbar\omega_0 = \gamma\hbar B_0$; for protons, the NMR frequency $\omega_0/2\pi B_0 = 42.58$ MHz/tesla. For N noninteracting protons per unit volume in thermal equilibrium the magnetization is $M_0 = N^2 B_0/k_B T$ in the limit $\mu B_0 \ll k_B T$. At room temperature, the magnetization is very small: for example, for protons at 300 K in 1 T, $M_0/N\mu \approx 3.4\times 10^{-6}$. When the field is reduced to, say, the earth's field ($\sim$50 μT), $M_0/N\mu \sim 10^{-10}$.

There is, however, one distinct advantage in performing NMR and MRI in very low fields. At a frequency of $\sim$1 GHz, to achieve a linewidth of 1 Hz, one must "shim" the magnet to achieve a field homogeneity of $1:10^9$ over the volume of the sample. At an NMR frequency of $\sim$1 kHz, on the other hand, one can achieve a 1-Hz linewidth with a homogeneity of $1:10^3$, which is relatively trivial to achieve. In the case of MRI, linewidth translates directly into spatial resolution: for a linewidth Δf in the absence of any applied field gradients, the spatial resolution in one dimension is $\Delta z = 2\pi\Delta f/\gamma G_z$, where G_z is the field gradient applied to perform frequency encoding.

How can one overcome the weak signal that is produced by the magnetic moment of the sample precessing in a small magnetic field? McDermott *et al.* [84] performed NMR in microtesla fields by combining prepolarization [86], [87] of the sample in a much higher field with detection of the precessing spins by means of a SQUID coupled to an untuned flux transformer. Thus, the signal from the SQUID becomes *independent* of the magnetic field B_0: the value of M_0 is determined by the initial polarizing field, and the flux coupled to the SQUID is proportional to the *flux*, rather than to the *rate of change* of flux. By contrast, in conventional NMR and MRI, by Faraday's law the voltage induced into an inductor scales as $\omega_0 M_0$ and hence as B_0^2.

For their first experiments, McDermott *et al.* used a liquid-helium-cooled, first-derivative gradiometer (Section IV-A); a double-walled glass dewar allowed a sample, maintained at room temperature by a heater, to be lowered into one of the pickup loops. After the polarizing field, typically 2 mT applied along the axis of the gradiometer, was rapidly switched off, the spins precessed about the measurement field B_0 of a few microtesla applied at right angles to the gradiometer axis, inducing an oscillating flux at frequency $\gamma B_0/2\pi$ into the SQUID. Subsequently, B_0 was abruptly reversed, causing the spins to precess in the opposite sense and forming a spin echo. The Fourier spectrum of the echo is the NMR line.

Fig. 12 illustrates the dramatic reduction in the linewidth obtained by reducing B_0. Fig. 12(a) shows the NMR spectrum of protons in mineral oil obtained with a constant field of 1.8 mT, averaged over 10 000 transients. The linewidth of about 1 kHz indicates that the inhomogeneity of B_0—which was produced by a quite small coil—was roughly 1%. By contrast, Fig. 12(b) shows the spectrum of the same sample—prepolarized in 2 mT—in a field of 1.8 μT produced by the same coil, averaged over 100 transients. The linewidth has been reduced by three orders of magnitude to about 1 Hz. Furthermore, the signal-to-noise ratio has been greatly enhanced over that in Fig. 12(a): since the area under the peak is conserved, the greatly reduced width results in a proportionately increased peak height. McDermott *et al.* used their technique to obtain the NMR spectrum of protons in trimethyl phosphate, where the electron mediated coupling of the ^{31}P nucleus to the nine equivalent protons splits their resonance into a doublet corresponding to their two possible spin orientations. The splitting of 10.4 $\pm$ 0.6 Hz

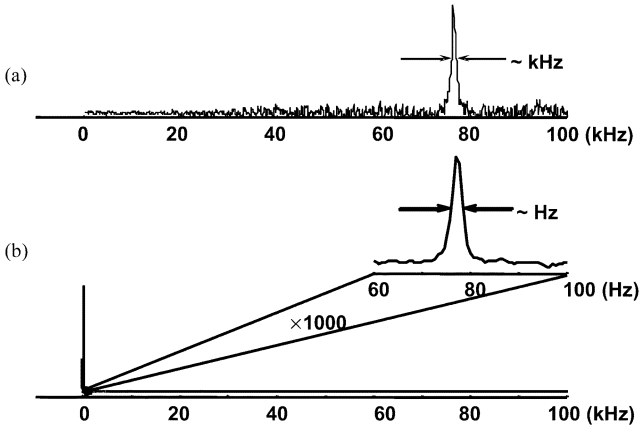

Fig. 12. NMR spectra of mineral oil. (a) Acquired in a static field of 1.8 mT, averaged 10 000 times. (b) Acquired in a static field of 1.8 μT using a field reversal echo following prepolarization at 2 mT, averaged 100 times. (From [84], with permission.)

was very well resolved. Because such scalar couplings are specific to a given covalent bond, this technique could be used to detect the presence of a given chemical.

McDermott *et al.* extended their microtesla NMR technique to MRI [85]. The flux transformer was configured as a second-derivative axial gradiometer (Section IV-A), with the lowest loop placed near the lower end of a low-noise fiberglass dewar; the sample was placed outside the dewar, close to the bottom. The static field, typically 132 μT, was applied along the z axis, perpendicular to the axis of the gradiometer (x direction). Three sets of gradient coils were used to apply the gradients $\partial B_z/\partial x, \partial B_z/\partial y$, and $\partial B_z/\partial z$ and a further coil supplied the polarizing field, typically 100–300 mT, along the x axis. The sample was placed at the center of a 2-m cube, which was equipped with three pairs of coils to cancel the earth's magnetic field. The cube was enclosed in a 3-mm-thick Al shield that attenuated ambient magnetic field fluctuations at the 5.6-kHz measurement frequency by an order of magnitude.

To obtain a 2-D image, the gradients $\partial B_z/\partial y$ and $\partial B_z/\partial z$ were stepped through successive values to rotate the resultant gradient through 48 steps. For each gradient, after the polarizing field was turned off, the spins reoriented along B_0 and a subsequent resonant pulse caused them to precess in the x–y plane. A second resonant pulse formed a spin echo, which was recorded. The image was obtained through projection reconstruction. An MRI "slice" was selected by means of a gradient pulse along the x direction. Fig. 13 shows the slice obtained from a whole pepper, with a spatial resolution of about 1 mm.

In an earlier, different approach, Seton *et al.* [77]–[83] used a SQUID with a tuned input circuit. The 30-turn pickup coil was connected in series with a tuning capacitor, the input coil of the SQUID, and a "Q-spoiler" [88]. The resonant frequency was 425 kHz. The Q-spoiler consisted of a series array of Josephson junctions. When an RF pulse was applied to initiate spin precession, the large current induced in the input circuit exceeded the critical current of the array, and the ensuing dissipation reduced Q to a low value. This

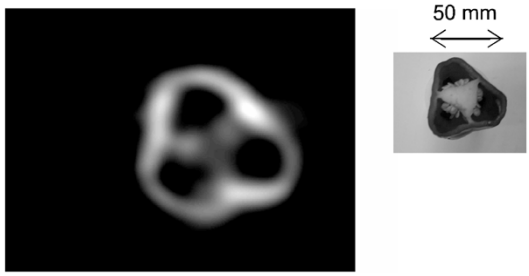

Fig. 13. MRI slice-selected image of a pepper obtained at 5.6 kHz with an untuned gradiometer. Photograph of the pepper, cut *after* the MRI, is on the right. (From [85], with permission.)

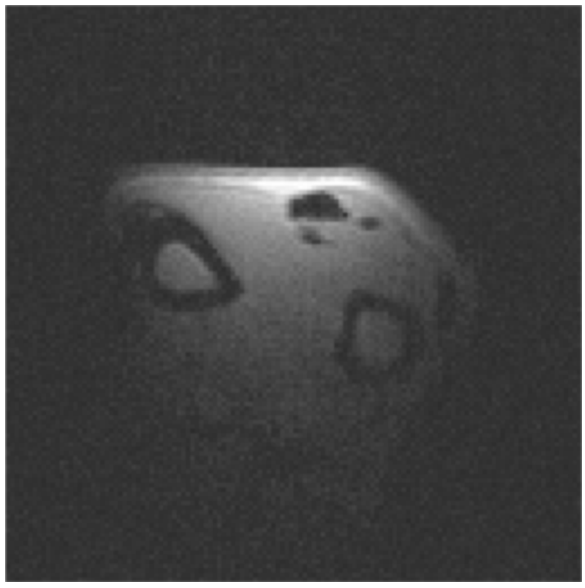

Fig. 14. MRI of the human forearm obtained at 425 kHz with a tuned SQUID gradiometer. (From [83], with permission).

technique enables one to achieve high Q-values—typically $Q \sim 30\,000$ in Seton's experiments—with a very short recovery time after the RF pulse has been turned off. The SQUID was operated in a direct-coupled FLL [33]. For the imaging experiments, the coil was deliberately damped to produce a $Q \sim 100$, thus extending the bandwidth to about 5 kHz. The noise of the resonant frequency was extraordinarily low, 0.08 fT $\cdot$ Hz$^{-1/2}$. This noise level is substantially lower than the noise of a conventional fiberglass dewar with aluminized mylar as the superinsulation, typically 3–5 fT $\cdot$ Hz$^{-1/2}$. Seton *et al.* achieved their much lower noise level in a custom-made dewar in which the upper cooled shield was made from an insulating ceramic and the superinsulation consisted of aluminized polyester. The fine structure of this material produces Al films with tiny particles that reflect well in the infrared while producing very low Nyquist noise currents. They obtained good-quality images of phantoms consisting of columns of water and of the human forearm [82]. Subsequently, to reduce the pickup of noise from the imaging coils, which are at room temperature, Seton *et al.* used a gradiometer to detect the NMR signal [83]. Using this system, they obtained an improved image of the forearm (Fig. 14) that clearly shows the radius and ulna.

It is interesting to compare the two approaches to MRI. The 425-kHz images demand a field homogeneity of about 2 ppm to achieve a 1-Hz linewidth. Although straightforward by the standards of high-field MRI, this homogeneity is much more demanding than the 200 ppm required by the 5.6-kHz system. The sensitivity of the tuned magnetometer is roughly 30 times better than the untuned magnetometer, but in the latter case, this difference is largely offset by the much higher effective magnetization due to prepolarization. Both approaches show considerable promise for clinical imaging of peripheral regions of the body such as the head, neck, and limb joints.

VI. Conclusion

Applications of SQUIDs continue to be dominated by low-T_c devices. The technology of Nb-based dc SQUIDs has not changed significantly over the last decade, signifying that their intrinsic noise suffices for most measurements. Indeed, the noise level is generally determined by environmental sources, except in those experiments where the SQUID and its signal source are enclosed in a superconducting shield. More development has occurred recently in the FLL, with the introduction of digital signal processors, particularly in multichannel biomagnetic systems. These systems continue to consume the majority of SQUIDs, and the market for them is growing steadily as the number of insurance-reimbursed procedures expands. The potential integration of low-field MRI with MSI in a single system is particularly intriguing, since all magnetic source images need to be superimposed on a magnetic resonance image for their interpretation.

The technology of high-T_c dc and RF SQUIDs on the other hand, is much less mature. Despite a concerted effort by the community, the development of a reproducible and reliable Josephson junction for operation at 77 K remains elusive. Furthermore, although several groups have demonstrated multilayer devices involving YBCO films, such structures have not been fabricated on a wafer scale. The lack of a flexible, bondable high-T_c wire is also a significant handicap. Thus, there is considerable scope for progress in high-T_c devices, particularly with regard to materials issues. Despite these difficulties, high-T_c SQUIDs are used in commercial products, notably for nondestructive evaluation, and thin-film magnetometers and gradiometers have sufficiently low noise for magnetocardiography. The introduction of a low-noise, relatively inexpensive cryocooler would have an enormous impact on the applicability of high-T_c SQUIDs, particularly if it operated at, say, 60 K where ramp-junctions become a viable proposition.

Space did not permit us to describe many applications of SQUIDs. One recent example is the use of low-T_c SQUIDs to measure the flux state of flux "qubits" involving one or three nanofabricated junctions connected in series on a superconducting loop [89], [90]. These experiments enable one to observe the superposition of quantum states in a macroscopic circuit, and to investigate the mechanisms for their relaxation and decoherence. Doubtless, there will be many more ingenious applications of these ultrasensitive flux detectors in the years to come.

References

[1] F. London, *Superfluids*. New York: Wiley, 1950.

[2] B. D. Josephson, "Possible new effects in superconductive tunneling," *Phys. Lett.*, vol. 1, pp. 251–253, 1962.

[3] R. C. Jaklevic, J. Lambe, A. H. Silver, and J. E. Mercereau, "Quantum interference effects in Josephson tunneling," *Phys. Rev. Lett.*, vol. 12, pp. 159–160, 1964.

[4] A. H. Silver and J. E. Zimmerman, "Quantum states and transitions in weakly connected superconducting rings," *Phys. Rev.*, vol. 157, pp. 317–341, 1967.

[5] J. G. Bednorz and K. A. Müller, "Possible high-T_c superconductivity in the Ba–La–Cu–O system," *Z. Phys. B, Condens. Matter*, vol. 64, pp. 189–193, 1986.

[6] H. Weinstock and R. W. Ralston, Eds., *The New Superconducting Electronics*. ser. NATO ASI series. Dordrecht, The Netherlands: Kluwer, 1993.

[7] H. Weinstock, Ed., *SQUID Sensors: Fundamentals, Fabrication and Applications*. Dordrecht, The Netherlands: Kluwer, 1996.

[8] H. Weinstock, Ed., *Applications of Superconductivity*. Dordrecht, The Netherlands: Kluwer, 2000.

[9] *SQUID Handbook*, J. Clarke and A. I. Braginski, Eds., Wiley–VCH, Berlin, Germany, 2004.

[10] V. Ambegaokar and B. I. Halperin, "Voltage due to thermal noise in the DC Josephson effect," *Phys. Rev. Lett.*, vol. 22, pp. 1364–1366, 1969.

[11] C. D. Tesche and J. Clarke, "DC SQUID: Noise and optimization," *J. Low Temp. Phys.*, vol. 29, pp. 301–331, 1977.

[12] ——, "DC SQUID: Current noise," *J. Low Temp. Phys.*, vol. 37, pp. 397–403, 1979.

[13] T. Ryhänen, H. Seppä, R. Ilimoniemi, and J. Knuutila, "SQUID magnetometers for low-frequency applications," *J. Low Temp. Phys.*, vol. 76, pp. 287–386, 1989.

[14] D. Koelle, R. Kleiner, F. Ludwig, E. Dantsker, and J. Clarke, "High-transition-temperature superconducting quantum interference devices," *Rev. Mod. Phys.*, vol. 71, pp. 631–686, 1999. *erratum, ibid.,* vol. 71, p. 1249, 1999.

[15] L. D. Jackel and R. A. Buhrman, "Noise in the RF SQUIDs," *J. Low Temp. Phys.*, vol. 19, pp. 201–246, 1975.

[16] G. J. Ehnholm, "Theory of the signal transfer and noise properties of the RF SQUID," *J. Low Temp. Phys.*, vol. 29, pp. 1–27, 1977.

[17] K. K. Likharev, *Dynamics of Josephson Junctions and Circuits*. New York: Gordon & Breach, 1986.

[18] P. K. Hansma, "Superconducting single-junction interferometers with small critical currents," *J. Appl. Phys.*, vol. 44, pp. 4191–4194, 1973.

[19] B. Chesca, "Theory of RF SQUIDS operating in the presence of large thermal fluctuations," *J. Low Temp. Phys.*, vol. 110, pp. 963–1002, 1998.

[20] R. Cantor and F. Ludwig, "SQUID fabrication technology," in *SQUID Handbook*, J. Clarke and A. I. Braginski, Eds, Berlin, Germany: Wiley–VCH, 2004, pp. 93–125.

[21] A. I. Braginski, H.-J. Krause, and J. Vrba, "SQUID magnetometers, superconducting film devices," in *Handbook of Thin Film Devices*, M. H. Francombe, Ed. New York: Academic, 2000, vol. 3, pp. 149–225.

[22] M. Gurvitch, M. A. Washington, and H. A. Huggins, "High-quality refractory Josephson tunnel junctions utilizing thin aluminum layers," *Appl. Phys. Lett.*, vol. 42, pp. 472–474, 1983.

[23] H. Hilgenkamp and J. Mannhart, "Grain boundaries in high-T_c superconductors," *Rev. Mod. Phys.*, vol. 74, pp. 485–549, 2002.

[24] F. Ludwig, E. Dantsker, D. Koelle, R. Kleiner, A. H. Miklich, and J. Clarke, "Multilayer magnetometers based on high-T_c SQUIDs," *Appl. Superconduct.*, vol. 3, pp. 383–398, 1995.

[25] A. I. Braginski, "Thin film structures," in *The New Superconducting Electronics*. ser. NATO ASI series, H. Weinstock and R. W. Ralston, Eds. Dordrecht, The Netherlands: Kluwer, 1993, pp. 89–122.

[26] F. C. Wellstood, J. J. Kingston, and J. Clarke, "Thin-film multilayer interconnect technology for $YBa_2Cu_3O_{7-x}$," *J. Appl. Phys.*, vol. 75, pp. 683–702, 1994.

[27] E. Dantsker, F. Ludwig, R. Kleiner, J. Clarke, M. Teepe, L. P. Lee, N. McN. Alford, and T. Button, "Addendum: Low noise YBCO-$SrTiO_3$-YBCO multilayers for improved superconducting magnetometers," *Appl. Phys. Lett.*, vol. 67, pp. 725–726, 1995.

[28] F. Ludwig, E. Dantsker, R. Kleiner, D. Koelle, J. Clarke, S. Knappe, D. Drung, H. Koch, N. McN. Alford, and T. W. Button, "Integrated high-T_c multiloop magnetometer," *Appl. Phys. Lett.*, vol. 66, pp. 1418–1420, 1995.

[29] M. I. Faley, U. Poppe, K. Urban, D. N. Paulsen, T. N. Starr, and R. L. Fagaly, "Low noise HTS DC-SQUID flip-chip magnetometers and gradiometers," *IEEE Trans. Appl. Superconduct.*, vol. 11, pp. 1383–1386, Mar. 2001.

[30] M. B. Ketchen and J. M. Jaycox, "Ultra-low noise tunnel junction DC SQUID with a tightly coupled planar input coil," *Appl. Phys. Lett.*, vol. 40, pp. 736–738, 1982.

[31] T. Ryhänen, H. Seppä, and R. Cantor, "Effect of parasitic capacitance and inductance on the dynamics and noise of DC superconducting quantum interference devices," *J. Appl. Phys.*, vol. 71, pp. 6150–6166, 1992.

[32] R. Cantor and D. Koelle, "Practical DC SQUIDs: Configuration and performance," in *SQUID Handbook*, J. Clarke and A. I. Braginski, Eds, Berlin, Germany: Wiley–VCH, 2004, pp. 171–217.

[33] D. Drung and M. Mück, "SQUID electronics," in *SQUID Handbook*, J. Clarke and A. I. Braginski, Eds, Berlin, Germany: Wiley–VCH, 2004, pp. 127–170.

[34] R. H. Koch, J. Clarke, W. M. Goubau, J. M. Martinis, C. M. Pegrum, and D. J. Van Harlingen, "Flicker $(1/f)$ noise in tunnel junction DC SQUIDs," *J. Low Temp. Phys.*, vol. 51, pp. 207–224, 1983.

[35] R. Cantor, V. Vinetskiy, and A. Matlashov, "A low-noise, integrated Dc SQUID magnetometer for applications in biomagnetism," in *Proc. Biomag 96*, C. J. Aine, Y. Okada, G. Stroink, S. J. Swithenby, and C. C. Wood, Eds., 2000, pp. 15–19.

[36] J. E. Zimmermann, "Sensitivity enhancement of superconducting quantum interference devices through the use of fractional-turn loops," *J. Appl. Phys.*, vol. 42, pp. 4483–4487, 1971.

[37] D. Drung, S. Knappe, and H. Koch, "Theory for the multiloop DC superconducting quantum interference device magnetometer and experimental verification," *J. Appl. Phys.*, vol. 77, pp. 4088–4098, 1995.

[38] D. Drung, S. Bechstein, K.-P. Franke, M. Schreiner, and T. Schurig, "Improved direct-coupled DC SQUID read-out electronics with automatic bias voltage tuning," *IEEE Trans. Appl. Superconduct.*, vol. 11, pp. 880–883, Mar. 2001.

[39] J. Vrba, "SQUID Gradiometers in Real Environments," in *SQUID Sensors: Fundamentals, Fabrication and Applications*, H. Weinstock, Ed. Dordrecht, The Netherlands: Kluwer, 1996, pp. 117–178.

[40] K. Barthel, D. Koelle, B. Chesca, A. I. Braginski, A. Marx, R. Gross, and R. Kleiner, "Transfer function and thermal noise of $YBa_2Cu_3O_{7-\delta}$ direct current superconducting quantum interference devices operated under large thermal fluctuations," *Appl. Phys. Lett.*, vol. 74, pp. 2209–2211, 1999.

[41] D. Drung, F. Ludwig, W. Müller, U. Steinhoff, L. Trahms, Y. Q. Shen, M. B. Jensen, P. Vase, T. Holst, T. Freltoft, and G. Curio, "Integrated $YB_2Cu_3O_{7-x}$ magnetometer for biomagnetic measurements," *Appl. Phys. Lett.*, vol. 68, pp. 1421–1423, 1996.

[42] D. Koelle, A. H. Miklich, F. Ludwig, E. Dantsker, D. T. Nemeth, and J. Clarke, "DC SQUID magnetometers from single layers of $YBa_2Cu_3O_{7-x}$," *Appl. Phys. Lett.*, vol. 63, pp. 2271–2273, 1993.

[43] L. P. Lee, J. Longo, V. Vinetskiy, and R. Cantor, "Low-noise $YBa_2Cu_3O_{7-x}$ direct-current superconducting quantum interference device magnetometer with direct signal injection," *Appl. Phys. Lett.*, vol. 66, pp. 1539–1541, 1995.

[44] J. Beyer, D. Drung, F. Ludwig, T. Minotani, and K. Enpuku, "Low-noise $YBa_2Cu_3O_{7-x}$ single layer DC superconducting quantum interference device (SQUID) magnetometer based on bicrystal junctions with 30° misorientation," *Appl. Phys. Lett.*, vol. 72, pp. 203–205, 1998.

[45] M. Mück, "Progress in RF-SQUIDs," *IEEE Trans. Appl. Superconduct.*, vol. 3, pp. 2003–2010, Mar. 1993.

[46] M. Mück, B. Chesca, and Y. Zhang, "Radio frequency SQUID's and their applications," in *Microwave Superconductivity*, H. Weinstock, Ed. Dordrecht, The Netherlands: Kluwer, 2001, pp. 505–540.

[47] A. I. Braginski and Y. Zhang, "Practical RF SQUID's and their applications," in *SQUID Handbook*, J. Clarke and A. I. Braginski, Eds, Berlin, Germany: Wiley–VCH, 2004, pp. 219–250.

[48] X. H. Zeng, Y. Zhang, B. Chesca, K. Barthel, Ya. S. Greenberg, and A. I. Braginski, "Experimental study of amplitude-frequency characteristics of high-transition-temperature radio frequency superconducting quantum interference devices," *J. Appl. Phys.*, vol. 88, pp. 7681–7687, 2000.

[49] B. Chesca, R. Kleiner, and D. Koelle, "SQUID theory," in *SQUID Handbook*, J. Clarke and A. I. Braginski, Eds, Berlin, Germany: Wiley–VCH, 2004, pp. 29–92.

[50] Y. Zhang, M. Mück, K. Herrmann, J. Schubert, W. Zander, A. I. Braginski, and C. Heiden, "Sensitive RF-SQUIDs and magnetometers operating at 77 K," *IEEE Trans. Appl. Superconduct.*, vol. 3, pp. 2465–2468, Mar. 1993.

[51] Y. Zhang, J. Schubert, N. Wolters, M. Banzet, W. Zander, and H.-J. Krause, "Substrate resonator for HTS RF SQUID operation," *Physica C*, vol. 372–376, pp. 282–286, 2002.

[52] H. R. Yi, Y. Zhang, J. Schubert, W. Zander, X. H. Zeng, and N. Klein, "Superconducting multiturn flux transformers for radio frequency superconducting quantum interference devices," *J. Appl. Phys.*, vol. 88, pp. 5966–5974, 2000.

[53] M. Mück, C. Heiden, and J. Clarke, "Investigation and reduction of low frequency excess noise in RF SQUIDs," *J. Appl. Phys.*, vol. 75, pp. 4588–4592, 1994.

[54] E. Dantsker, S. Tanaka, and J. Clarke, "High-T_c superconducting quantum interference devices with slots or holes: Low $1/f$ noise in ambient magnetic fields," *Appl. Phys. Lett.*, vol. 70, pp. 2037–2039, 1997.

[55] R. H. Koch, J. Z. Sun, V. Foglietti, and W. J. Gallagher, "Flux dam, a method to reduce extra low frequency noise when a superconducting magnetometer is exposed to a magnetic field," *Appl. Phys. Lett.*, vol. 67, pp. 709–711, 1995.

[56] J. Zmuidzinas and P. L. Richards, "Millimeter-wave detection and mixing," *Proc. IEEE*, vol. 92, pp. 1597–1616, Oct. 2004.

[57] G. L. Romani, C. Del Gratta, and V. Pizzella, "Neuromagnetism and its clinical applications," in *SQUID Sensors: Fundamentals, Fabrication, and Applications*, H. Weinstock, Ed. Dordrecht, The Netherlands: Kluwer, 1996, ch. ch. 11, pp. 445–490.

[58] S. E. Erné and J. Lehmann, "Magnetocardiography, an introduction," in *SQUID Sensors: Fundamentals, Fabrication and Applications*, H. Weinstock, Ed. Dordrecht, The Netherlands: Kluwer, 1996, pp. 395–412.

[59] G. Stroink, M.J.R. Lamothe, and M. J. Gardner, "Magnetocardiographic and electrocardiographic mapping studies," in *SQUID Sensors: Fundamentals, Fabrication and Applications*, H. Weinstock, Ed. Dordrecht, The Netherlands: Kluwer, 1996, pp. 413–444.

[60] W. Weitschies, R. Kötitz, R. Bunte, and L. Trahms, "Determination of relaxing or remanent nanoparticle magnetization provides a novel binding-specific technique for the evaluation of immunoassays," *Pharm. Pharmacol. Lett.*, vol. 7, pp. 1–7, 1997.

[61] R. Kötitz, W. Weitschies, L. Trahms, W. Brewer, and W. Semmler, "Determination of the binding reaction between avidin and biotin by relaxation measurements of magnetic nanoparticles," *J. Magn. Magn. Mater.*, vol. 194, pp. 62–68, 1999.

[62] Y. R. Chemla, H. L. Grossman, Y. Poon, R. McDermott, R. Stevens, M. D. Alper, and J. Clarke, "Ultrasensitive magnetic biosensor for homogeneous immunoassay," *Proc. Nat. Acad. Sci.*, vol. 97, pp. 14 268–14 272, 2000.

[63] H. L. Grossman, W. R. Myers, V. J. Vreeland, R. Bruehl, M. D. Alper, C. R. Bertozzi, and J. Clarke, "Detection of bacteria in suspension using a superconducting quantum interference device," *Proc. Nat. Acad. Sci.*, vol. 101, no. 1, pp. 129–134, 2004.

[64] K. Enpuku, T. Minotani, T. Gima, Y. Kuroki, Y. Itoh, M. Yamashita, Y. Katakura, and S. Kuhara, "Detection of magnetic nanoparticles with superconducting quantum interference device (SQUID) magnetometer and application to immunoassays," *Jpn. J. Appl. Phys.*, vol. 38, pp. L1102–L1105, 1999.

[65] D. V. Berkov and R. Kötitz, "Irreversible relaxation behavior of a general class of magnetic systems," *J. Phys., Condens. Matter*, vol. 8, pp. 1257–1266, 1996.

[66] C. Hilbert and J. Clarke, "DC SQUID's as radiofrequency amplifiers," *J. Low Temp. Phys.*, vol. 61, pp. 263–280, 1985.

[67] R. Bradley, J. Clarke, D. Kinion, L. J. Rosenberg, K. van Bibber, S. Matsuki, M. Mück, and P. Sikivie, "Microwave cavity searches for dark-matter axions," *Rev. Mod. Phys.*, vol. 75, pp. 777–817, 2003.

[68] M. A. Tarasov, V. Yu. Belitsky, and G. V. Prokopenko, "DC SQUID RF amplifiers," *IEEE Trans. Appl. Superconduct.*, vol. 2, pp. 79–83, June 1992.

[69] M. Mück, M.-O. André, J. Clarke, J. Gail, and C. Heiden, "Radio frequency amplifier based on a niobium DC superconducting quantum interference device with microstrip input coupling," *Appl. Phys. Lett.*, vol. 72, pp. 2885–2887, 1998.

[70] ——, "The microstrip superconducting quantum interference device RF amplifier: Tuning and cascading," *Appl. Phys. Lett.*, vol. 75, pp. 3545–3547, 1999.

[71] M.-O. André, M. Mück, J. Clarke, J. Gail, and C. Heiden, "Microstrip DC superconducting quantum interference device radio-frequency amplifier with tenth-kelvin noise temperature," *Appl. Phys. Lett.*, vol. 75, pp. 698–700, 1999.

[72] M. Mück, J. B. Kycia, and J. Clarke, "Superconducting quantum interference device as a near-quantum-limited amplifier at 0.5 GHz," *Appl. Phys. Lett.*, vol. 78, pp. 967–969, 2001.

[73] R. J. Schoelkopf, P. Wahlgren, A. A. Kozhevnikov, P. Delsing, and D. E. Prober, "The radio-frequency single-electron transistor (RF-SET): A fast and ultrasensitive electrometer," *Science*, vol. 280, pp. 1238–1242, 1998.
[74] C. P. Slichter, *Principles of Magnetic Resonance*, 3rd ed. New York: Springer-Verlag, 1989.
[75] E. M. Haacke, R. W. Brown, M. R. Thompson, and R. Venkatesan, *Magnetic Resonance Imaging: Physical Principles and Sequence Design*. New York: Wiley, 1999.
[76] Ya. S. Greenberg, "Application of superconducting quantum interference devices to nuclear magnetic resonance," *Rev. Mod. Phys.*, vol. 70, pp. 175–222, 1998.
[77] H. C. Seton, D. M. Bussel, J. M. S. Hutchison, I. Nicholson, and D. J. Lurie, "DC SQUID based NMR detection from room temperature samples," *Phys. Med. Biol.*, vol. 37, pp. 2133–2138, 1992.
[78] H. C. Seton, D. M. Bussel, J. M. S. Hutchison, and D. J. Lurie, "Use of a DC SQUID receiver preamplifier in a low field MRI system," *IEEE Trans. Appl. Superconduct.*, vol. 5, pp. 3218–3221, 1995.
[79] H. C. Seton, D. M. Bussel, and J. M. S. Hutchison, "A DC SQUID RF amplifier used in low field MRI system," in *Proc. 2nd Eur. Conf. Applied Superconductivity*, D. Dew-Hughes, Ed., 1995, pp. 1487–1490.
[80] ——, "A liquid helium cooled RF coil and SQUID amplifier for MRI at 0.01 T," in *Proc. Society of Magnetic Resonance*, vol. 2, 1995, p. 959.
[81] ——, "A tuned SQUID amplifier for MRI based on a DOIT flux locked loop," *IEEE Trans. Appl. Superconduct.*, vol. 7, pp. 3213–3216, June 1997.
[82] H. C. Seton, J. M. S. Hutchison, and D. M. Bussel, "A 4.2 K receiver coil and SQUID amplifier to improve the SNR of low-field magnetic resonance images of the human arm," *Meas. Sci. Technol.*, vol. 8, pp. 198–207, 1997.
[83] ——, "Gradiometer pick-up coil design for a low-field SQUID-MRI system," *Magn. Reson. Mater. Phys., Biol. Med. (MAGMA)*, vol. 8, pp. 116–120, 1999.
[84] R. McDermott, A. H. Trabesinger, M. Mück, E. L. Hahn, A. Pines, and J. Clarke, "Liquid state NMR and scalar couplings in microtesla magnetic fields," *Science*, vol. 295, pp. 2247–2249, 2002.
[85] R. McDermott, N. Kelso, S.-K. Lee, M. Mößle, M. Mück, W. Myers, B. ten Haken, H. C. Seton, A. H. Trabesinger, A. Pines, and J. Clarke, "SQUID-detected magnetic resonance imaging in microtesla magnetic fields," *J. Low Temp. Phys.*, vol. 135, no. 5–6, pp. 793–821, June 2004.
[86] A. Macovski and S. Connolly, "Novel approaches to low cost MRI," *Magn. Reson. Med.*, vol. 30, pp. 221–230, 1993.
[87] J. Stepišnik, V. Eržen, and M. Kos, "NMR imaging in the earth's magnetic field," *Magn. Reson. Med.*, vol. 15, pp. 386–391, 1990.
[88] C. Hilbert, J. Clarke, T. Sleator, and E. L. Hahn, "Nuclear quadrupole resonance detected at 30 MHz with a DC SQUID," *Appl. Phys. Lett.*, vol. 47, pp. 637–639, 1985.
[89] J. R. Friedman, V. Patel, W. Chen, S. K. Tolpygo, and J. E. Lukens, "Quantum superposition of distinct macroscopic states," *Nature*, vol. 406, pp. 43–46, 2000.
[90] I. Chiorescu, Y. Nakamura, C. J. P. M. Harmans, and J. E. Mooij, "Coherent quantum dynamics of a superconducting flux qubit," *Science*, vol. 299, pp. 1869–1871, 2003.

Reinhold Kleiner was born in Thannhausen, Germany on May 16, 1962. He received the Ph.D. degree from the Technical University of Munich, Munich, Germany, in 1992 and the Habilitation degree from the University of Erlangen-Nürnberg in 1997.

From 1994 to 1995, he was with J. Clarke's Group at the University of California, Berkeley, as a Guest Researcher, and subsequently became Assistant Professor in the Physics Institute, University of Erlangen-Nürnberg, Nürnberg, Germany. In 2000, he was appointed Full Professor for Experimental Solid-State Physics at the University of Tübingen, Tübingen, Germany. He has also been engaged as Vice Dean, Faculty of Mathematics and Physics, since 2002. His scientific interests include high- and low-temperature superconductivity, magnetic and superconducting layered materials, superconducting quantum interferometry, Josephson effects, nonlinear dynamics, and imaging techniques at low temperatures.

Dieter Koelle was born in Merklingen, Germany on September 25, 1960. He received the Ph.D. degree in physics from the University of Tübingen, Tübingen, Germany, in 1992 and the Habilitation degree from the University of Cologne in 1999.

From 1992 to 1994, he was with J. Clarke's group at the University of California, Berkeley, as a Guest Researcher, returning to Tübingen in 1995. Subsequently, he became a Research Assistant, University of Cologne, Cologne, Germany (1996–2001). During the same period, he also served as a Scientific Adviser at the Forschungszentrum Jülich, ISI, Jülich, Germany. In 2001, he was appointed Professor for Experimental Solid State Physics at the University of Tübingen. His research activities are mainly devoted to superconductivity with focus on cuprate high-T_c superconductors and other perovskite-oxides, for example, manganites. His scientific interests include thin-film technology, imaging techniques at low temperatures (scanning electron microscopy and scanning laser microscopy), order parameter symmetry in unconventional superconductors, Josephson junctions, superconducting quantum interference devices, superconducting transistors, and ratchet effects in superconductors.

Frank Ludwig received the Ph.D. degree from the Humboldt University, Berlin, Germany, in 1987 for his magnetooptical investigations of the two-dimensional electron gas at InSb grain boundaries.

From 1987 to 1992, he was a Research and Teaching Assistant, Physics Department, Humboldt University. From 1992 to 1995, he was a Research Associate at the University of California, Berkeley, with J. Clarke, working on the development of highly sensitive high-T_c superconducting quantum interference device (SQUID) magnetometers. From 1995 to 2001, he was a Researcher in the Cryosensors Laboratory at the Physikalisch Technische Bundesanstalt, Berlin, where he continued his work on the development and fabrication of high-T_c SQUID magnetometers with emphasis on their operation in magnetically disturbed environments. Since 2001, he has been carrying out research and teaching at the Institut für Elektrische Messtechnik und Grundlagen der Elektrotechnik, Technical University Braunschweig, Braunschweig, Germany. His scientific activities are focussed on the development of highly sensitive SQUID and flux gate magnetometers, and their implementation in systems, for example, for medical and biological investigations.

John Clarke received the B.A., M.A. Ph.D., and Sc.D. degrees in physics from the University of Cambridge, Cambridge, U.K. in 1964, 1968, and 2003, respectively.

From 1968 to 1969, he was a Postdoctoral Scholar at the University of California, Berkeley. He has been a Faculty Member of the Physics Department since 1969 and is also a Faculty Senior Scientist at Lawrence Berkeley National Laboratory, Berkeley. His research interests include fundamental aspects of superconductivity, and the development and application of low- and high-transition-temperature superconducting quantum interference devices to a broad range of problems, including low-frequency nuclear magnetic resonance and magnetic resonance imaging, decoherence in mesoscopic circuits, biosensors, and axion detectors.

Prof. Clarke is a Fellow of the Royal Society. He was the recipient of the Keithley Award of the American Physical Society in 1998, the Comstock Prize in Physics of the National Academy of Sciences in 1999, and the IEEE Council on Superconductivity Award in 2002.